Accepted Manuscript

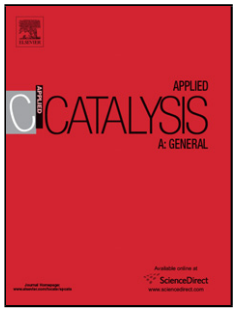

Title: The catalytic cracking of sterically challenging plastic feedstocks over high acid density Al-SBA-15 catalysts

Authors: Joseph Socci, Amin Osatiashtiani, Georgios Kyriakou, Tony Bridgwater

PII: S0926-860X(18)30575-1
DOI: https://doi.org/10.1016/j.apcata.2018.11.020
Reference: APCATA 16889

To appear in: *Applied Catalysis A: General*

Received date: 17 September 2018
Revised date: 21 November 2018
Accepted date: 23 November 2018

Please cite this article as: Socci J, Osatiashtiani A, Kyriakou G, Bridgwater T, The catalytic cracking of sterically challenging plastic feedstocks over high acid density Al-SBA-15 catalysts, *Applied Catalysis A, General* (2018), https://doi.org/10.1016/j.apcata.2018.11.020

The catalytic cracking of sterically challenging plastic feedstocks over high acid density Al-SBA-15 catalysts

Joseph Socci, Amin Osatiashtiani, Georgios Kyriakou, Tony Bridgwater*

European Bioenergy Research Institute (EBRI), School of Engineering and Applied Science, Aston University, Aston Triangle, Birmingham, B4 7ET, United Kingdom.

* Corresponding Author: a.v.bridgwater@aston.ac.uk

Graphical Abstract

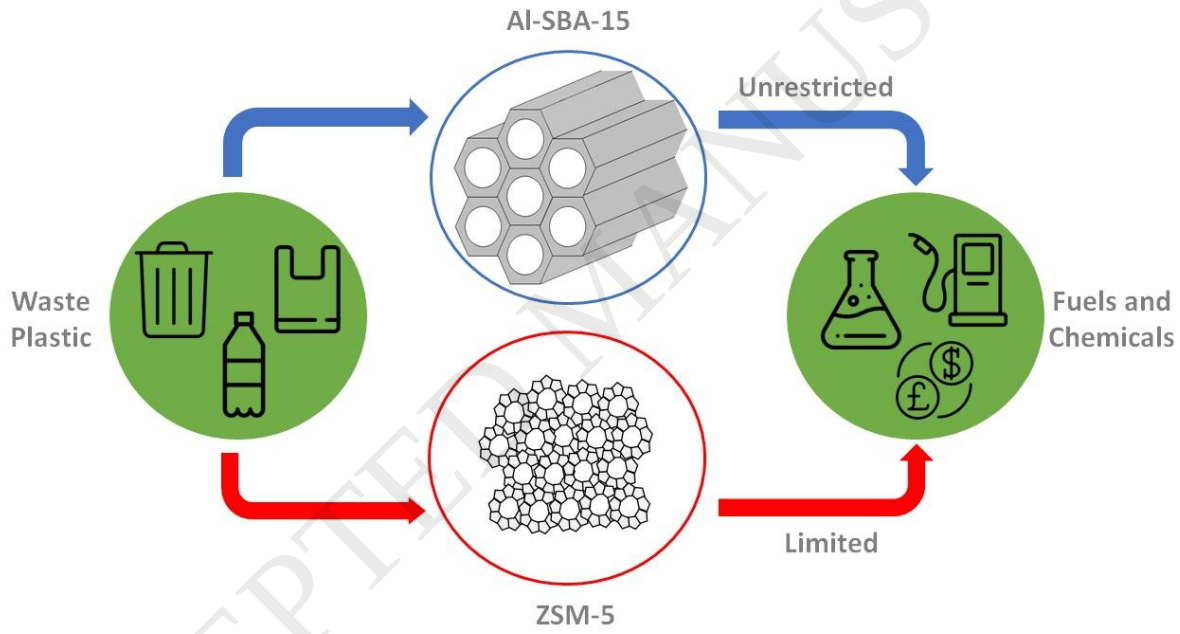

Highlights

- Synthesis of Al-SBA-15 catalysts with similar acidic properties to zeolites.
- Al-SBA-15 catalysts overcomes diffusional limitations of ZSM-5 in LDPE cracking.
- Aluminium rich SBA-15 exhibits high selectivity to gasoline range hydrocarbons.
- Selectivity can be fine-tuned by controlling the incorporation of Al into SBA-15.

Abstract

The catalytic cracking of polyolefinic waste materials over solid acid catalysts, such as zeolites, is a promising process for the production of useful fuels and chemicals. However, the inherent diffusional constraints of the microporous zeolites restrict the access of bulky polyolefin molecules to the active site, therefore limiting their effectiveness. To address this, a simple yet effective method of producing mesoporous Al-SBA-15 materials with a high density of Brønsted acid sites has been employed. These catalysts are shown to be very active for the catalytic cracking of low density polyethylene (LDPE), a common waste plastic. The acidic and textural properties of the catalysts were characterised by ICP-OES, XPS, XRD, N_2 physisorption, propylamine-TPD, pyridine-FTIR and STEM and have been correlated with their catalytic activity. The product distribution from the catalytic cracking of LDPE has been shown to depend strongly on both the pore architecture and the Al content of the SBA-15 and thus the density and strength of Brønsted acid sites. Fine-tuning the Al content of the SBA-15 materials can direct the product distribution of the hydrocarbons. The Al-SBA-15 materials display increased cracking orientated towards aliphatic hydrocarbons compared to ZSM-5, attributed to the mesoporous nature of SBA-15, overcoming diffusional limitations.

Keywords: Mesoporous materials, Al-SBA-15, Catalytic cracking, LDPE, Pyrolysis

1. Introduction

The catalytic cracking of polyolefin waste for the production of transportation fuels and chemicals is receiving increased attention due to the environmental and economic benefit associated with these technologies [1].

Several studies have been carried out to examine the catalytic cracking of pure polyolefins over solid acid catalysts such as zeolites, clays and ordered mesoporous materials (OMMs) including MCM-41 and SBA-15 [2–4]. Typically, high catalytic activity is observed with materials possessing high acid strength/densities, high surface areas and large pore sizes which facilitate the accessibility of bulky plastic derivatives to the active sites [5].

Zeolites possess high stability and strong acidity due to their highly crystalline framework and have been employed industrially in large-scale applications such as in refining and petrochemistry [6]. However, their microporous nature presents severe mass transfer limitations of the bulky polyolefin derivatives to the internal pores, where the majority of the acid sites can be found. Contrary to this, silica (SiO_2) based mesoporous materials, such as MCM-41 and SBA-15, possess an ordered arrangement of pores with diameters between 2 and 50 nm compared to 0.5 nm for ZSM-5. This overcomes the limitation of diffusional constraints associated with microporous zeolites. However, the application of MCM-41 is limited in many catalytic processes due to its relatively low thermal and hydrothermal stability compared to zeolites and alumina [7]. Mesoporous silica SBA-15 is structurally very similar to

MCM-41 but has thicker pore walls (4-8 nm compared to 1-2 nm for MCM-41) and larger pore sizes (2-15 nm compared to 2-5 nm for MCM-41) [8]. The thicker pore walls of SBA-15 results in improved framework crosslinking compared to MCM-41, leading to higher thermal and hydrothermal stability. These properties have opened up many new opportunities in separation, adsorption, as drug delivery carriers and as heterogeneous catalysts [9–12].

The insertion of aluminium ions into the SBA-15 structure allows the creation of acid sites which are essential for acid catalysed reactions. However, it is difficult to achieve high levels of aluminium incorporation into Al-SBA-15, due to the difference in hydrolysis rates of Al and Si at the low pH required for SBA-15 synthesis [13]. Various synthetic methods have been proposed for the incorporation of higher amounts of aluminium to achieve higher surface acidities [14–16]. A literature survey on the acidity evaluation for a variety of Al-SBA-15 synthesis methods is presented in Table 1.

Table 1. Comparison of Al-SBA-15 synthesis and acidity evaluation referenced in literature. References are presented in chronological order.

Author	Year	Ref.	Al incorporation	Lowest Si/Al	Acidity (μmol/g)	Brief evaluation
Luan et al.	1999	[17]	Direct synthesis	8.5	N/A	Acidity not evaluated.
Sumiya et al.	2001	[18]	Post synthesis	4.8	N/A	Py-IR confirms existence of Brønsted acid sites and confirmed by cumene cracking reaction, though not quantified.
Y. Li et al.	2004	[13]	Direct synthesis/two step	22	N/A	Py-IR shows increase in Brønsted and Lewis acidity with a decrease in Si/Al, not quantified.
S. Wu et al.	2004	[16]	pH adjustment	2.4	N/A	Acid sites not measured.
Zeng et al.	2005	[19]	Post synthesis	7.2	430	Acidity quantified by Py-IR, highest Brønsted acidity achieved at Si/Al = 9.8 (81.2 μmol g^{-1}).
W. Hu et al.	2006	[20]	Post synthesis	10	160	Acid sites evaluated by probe molecules and NMR. Acid site strength is dependent on the probe molecule.
Van Grieken et al.	2006	[21]	pH adjustment	31	110	Acid properties measured by NH_3 TPD, shows acidity is 0.11 mequiv.NH_3 g^{-1} (Si/Al = 30).
Muthu Kumaran et al.	2008	[22]	Direct synthesis	11.4	402	Acidity evaluated by NH_3, linear relationship between acidity and cumene cracking. Highest total acidity achieved at Si/Al = 11 (402 μmol g^{-1}).
Dragoi et al.	2009	[23]	Direct and post synthesis	8	491	Acidity evaluated by both Py-IR and NH_3 TPD, highest acidity achieved at Si/Al = 8 (470 and 491 μmol g^{-1}, Py-IR and NH_3 TPD respectively).
Gallo et al.	2010	[24]	pH adjustment and post synthesis	13.2	417	Acidity quantified and evaluated by Py-IR and NH_3 TPD, highest Brønsted acidity achieved with post synthesis method. Si/Al = 15 (128 and 622 μmol g^{-1}, Py-IR and NH_3 TPD respectively).

Bhange et al.	2011	[25]	Direct synthesis	20	440	Acidity quantified by NH3 TPD. Highest total acidity was seen at Si/Al = 20 (440 µmol g^{-1}) decreasing Si/Al decreased quantity of Brønsted sites.
Koekkoek et al.	2012	[26]	Direct synthesis	14	4	Acidity evaluated by the catalytic activity of n-heptane conversion. Highest Brønsted acidity at Si/Al = 14 (3.6 µmol g^{-1}).
Ungureanu et al.	2012	[27]	pH adjustment	5.2	471	Acidity quantified and evaluated by Py-IR, no difference in Brønsted/Lewis ratios with Al incorporation.
S. Lin et al.	2015	[28]	Direct synthesis	34	2960	Acidity quantified and evaluated by NH_3 TPD, highest total acidity at Si/Al = 34 (2960 µmol g^{-1}).
Meloni et al.	2016	[29]	pH adjustment	3.4	438	Acidity evaluated by NH_3 TPD, highest total acidity at Si/Al = 3.4 (438 µmol g^{-1}).
Xing et al.	2017	[30]	Direct synthesis	13	58	Acidity evaluated by Py-IR, highest Brønsted acidity achieved at Si/Al = 13 (58 µmol g^{-1}).
Socci et al.	2018	This paper	pH adjustment	5	564	Acidity quantified by propylamine -TPD and evaluated by Py-IR.

According to the literature, the quality of aluminium incorporation for the generation of acid sites is highly dependent on the synthesis procedure. The direct synthesis of Al-SBA-15 results in Al species that are not retained in the silica framework and often end up as extra-framework aluminium. Likewise, post-synthesis techniques require additional preparation steps and further calcination also leading to a high amount of extra-framework aluminium [24]. On the other hand, the “pH adjustment” method is a simple, but effective, technique for the incorporation of high amounts of aluminium (Si/Al = < 25) into SBA-15, with high Brønsted acidity, similar to those found in zeolites [27]. Furthermore, results for the characterisation and quantification of acidic sites can vary between methods. Therefore, caution must be taken when comparing values measured by different techniques [31].

Structural/textural properties are also heavily dependent on Al-SBA-15 synthesis parameters such as ageing temperature and time: generally higher temperatures and longer hydrothermal treatment steps lead to larger mesopore pore diameters and higher surface areas [32]. Previous work reported on the catalytic activity of Al-SBA-15 catalysts, for the cracking of waste plastics, have either used direct synthesis methods or post-synthesis grafting at medium Si/Al ratios which are unable to yield large quantities of aluminium in the tetrahedral environment. This has led to an unreasonable comparison of both the catalytic activity and distribution of products by OMMs, in the cracking of waste polyolefins, with much lower acidities compared to that of zeolites [5,33,34].

Polyolefin plastics in particular, low density polyethylene (LDPE) in Fig. 1, accounts for the majority of plastics consumed and find use in many applications, such as packaging and

insulation [1]. The catalytic cracking of polyolefins proceeds through the formation of a carbonium ion or carbenium ion upon reaction with a Brønsted or Lewis acid site, respectively [35]. Following this, several other acid-catalysed reactions may occur on the acid sites such as isomerisation, oligomerisation, cyclisation, aromatisation and further cracking [1]. The numerous side branches of varying chain length, present in LDPE, cause its low density and low amounts of crystallinity compared to high density polyethylene (HDPE). Furthermore, although the presence of side branches in LDPE facilitates cracking through the formation of tertiary carbocations, the existence of cross-linking in LDPE reduces cracking rates compared to HDPE. This is likely due to steric hindrances which limits access to active sites of the catalyst [36].

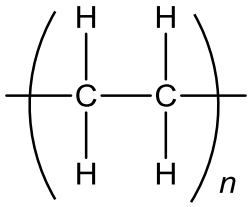

Fig. 1. Repeatable monomer of low density polyethylene (LDPE).

In this work, a series of Al-SBA-15 catalysts have been synthesised with Si/Al ranging from (100-5:1), using the alternative "pH adjustment" method, in order to produce acidities comparable to zeolites. The newly-created catalysts were characterised by ICP-OES, XPS, XRD, N_2 physisorption, propylamine-TPD, pyridine-FTIR and STEM. They were subsequently applied in the catalytic cracking of the sterically challenging feedstock LDPE, to investigate the relationship between their physicochemical properties and their cracking effectiveness. The catalytic properties of the Al-SBA-15 materials were compared to those of microporous ZSM-5 catalyst in order to assess diffusion limitations and reactant accessibility of the active sites.

2. Experimental methods

2.1 Chemicals and Materials

Pluronic P123 (M_n= 5800, $EO_{20}PO_{70}EO_{20}$), tetraethyl orthosilicate (TEOS, >98%), Al $(NO_3)_3{\cdot}9H_2O$ (>98%), hydrochloric acid (37 wt. %) and ammonium hydroxide solution (28-30% NH_3 basis) were all purchased from Sigma-Aldrich. ZSM-5 (SM-27 (Si/Al=12) reference material was purchased from Alsi-Penta Zeolithe GmbH. LDPE was kindly supplied by Sabic Europe.

2.2 Synthesis of SBA-15

SBA-15 was synthesised following the procedure reported by Zhao and co-workers [37]. Approximately 4 g of Pluronic P123 triblock copolymer was dissolved in 125 ml of 2 M HCl

solution and stirred at 35 °C for 4 h. 8.5 ml of TEOS was added dropwise and left stirring for a further 20 h. The resulting gel was aged at 100 °C for 48 h. The solid product was separated by vacuum filtration, washed with water and dried at 60 °C, then heated to 550 °C at a ramp rate of 1.5 °C min^{-1} and held for 6 h.

2.3 Incorporation of aluminium

A series of Al-SBA-15 catalysts was synthesised with Si/Al ratios ranging from 100:1 to 5:1 using a modified two-step "pH adjustment method" developed by Wu and co-workers [16]. The method was modified by using $Al(NO_3)_3{\cdot}9H_2O$ as the aluminium source instead of $Al_2(SO_4)_3{\cdot}18H_2O$; as well as incorporating a longer hydrothermal treatment in the second step (72 h instead of 48 h to increase the pore size) [27]. Approximately 4 g of Pluronic P123 triblock copolymer was dissolved in 125 ml of 2 M HCl solution and stirred at 35 °C for 4 h. 8.5 ml of tetraethyl orthosilicate (TEOS) was added dropwise and left to stir for 3 h. Then, the amount of $Al(NO_3)_3{\cdot}9H_2O$ required to give the specific Si/Al ratio was added to the mixture and left to stir for 20 h. The resulting gel was aged at 100 °C for 48 h before being cooled to room temperature. The pH value of the mixture was increased to 7.5 by the dropwise addition of 4 M NH_4OH with stirring, and the mixture was then subjected to a second hydrothermal treatment at 100 °C for 72 h. The solid product was separated by vacuum filtration, washed with water and dried at 60 °C, before being calcined in static air at a ramp rate of 1.5 °C min^{-1} to 550 °C with a hold time of 6 h. The resulting Al-SBA-15 materials were designated as AlSBA15(X), where X indicates the molar Si/Al ratio in the synthesised catalyst.

2.4 Materials Characterisation

Low angle X-ray diffraction patterns were recorded for 2θ = 0.5-5° with a step size of 0.01, on a Bruker D8 Advance diffractometer fitted with an X'celerator and Cu K_α (1.54 Å) radiation source and nickel filter.

The Si and Al contents of the bulk of the samples were determined by ICP-OES on a Thermo Scientific iCAP 7000 instrument. Prior to analyses, samples were digested in a mixture of nitric acid, sulphuric acid and deionised water using a CEM SP-D discover microwave (300 W). Ammonium fluoride was added to generate hydrofluoric acid in-situ before neutralisation with boric acid and HCl. The samples were subsequently diluted with deionised water by a factor of 10.

XPS analysis was carried out on a Kratos Supra employing a monochromated Al Kα X-ray source (hv = 1486.7 eV). The data was processed using CasaXPS version 2.3.14, with binding energies corrected to the C 1s peak at 284.6 eV and surface compositions quantified by application of element and instrument specific response factors.

Nitrogen physisorption analyses were measured at -196 °C on a Quantachrome Nova 4000 porosimeter and analysed with NovaWin software. Samples were degassed under vacuum at 120 °C for 10 h prior to analysis. Surface areas (***S***) were calculated using the Brunauer, Emmet Teller (BET) model and the de Boer "t-plot" method was applied to calculate the micropore volume (V_μ). The single point gas adsorption volume (V_T) was calculated using the amount of gas adsorbed at a relative pressure of 0.98 in the desorption branch using the Barrett, Joyner and Halenda (BJH) method. The volume of the mesopores (V_m) was calculated using the equation $V_m = V_T - V_\mu$. The BJH method was also applied to the adsorption branch to calculate mean pore diameters (d_p).

Acid site densities were determined by propylamine adsorption followed by thermogravimetric analysis coupled with mass spectrometry (TGA-MS), where chemisorbed propylamine decomposes into propene and ammonia over acid sites. Prior to analyses, propylamine was added dropwise to samples and then excess physisorbed propylamine was removed by vacuum drying at 35 °C overnight. Temperature programmed desorption was performed on a Mettler Toledo TGA/DSC 2 StarSystem between 40 and 800 °C under a He flow of 20 ml min^{-1}, using a ramp rate of 10 °C min^{-1}. Propene and ammonia were detected using a Pfeiffer Vacuum, ThermoStar MS at m/z = 41 and 17 respectively.

The Brønsted/Lewis acid character of the catalysts was studied by means of Diffuse Reflectance Infrared Fourier Transform Spectroscopy (DRIFTS) using pyridine as a probe molecule. Ex-situ pyridine adsorption was performed by the saturation of diluted samples (10 wt. % in KBr). Excess physisorbed pyridine was removed under vacuum at 35 °C prior to spectral acquisition on a Thermo Scientific Nicolet iS50 FT-IR spectrometer with a mercury cadmium telluride (MCT-A) photo detector at -196 °C, cooled by liquid nitrogen. Analyses were performed in an environmental cell at 110 °C, to remove physisorbed water/moisture.

High-resolution S/TEM images were taken using an FEI Philips TECNAI F20 at 200 kV equipped with an Oxford instruments ISIS Energy Dispersive Spectroscopy (EDS) detector, located at The Centre for Electron Microscopy, University of Birmingham. The sample was diluted in ethanol and then deposited by drop casting onto a carbon coated mesh copper grid and then dried under ambient conditions.

2.5 Catalytic Cracking of LDPE

2.5.1 Thermogravimetric Analysis

Both thermal and catalytic cracking of LDPE was investigated using a Perkin-Elmer Pyris 1 thermogravimetric analyser (TGA) equipped with a 20 position autosampler. The powdered polymer and powdered catalyst, with similar particle sizes (2-10 μm), were thoroughly mixed using a mortar and pestle in a weight ratio of LDPE:catalyst = 3:1. Then, 5 mg of the sample mixture was loaded into the ceramic crucibles for analysis. The sample was heated from 50

to 600 °C at 10 °C min^{-1}, under a nitrogen inert atmosphere with a flow rate of 20 ml min^{-1}. Each experiment was performed in triplicate and an average of the measured values was calculated and presented on a percentage conversion basis (Eq. 1).

Eq. 1 $$Conversion\ (\%) = \frac{Initial\ LDPE\ mass - Final\ mass}{Initial\ LDPE\ mass} \times 100$$

2.5.2 Py-GC/MS Analysis

The selectivity of the thermal and catalytic cracking of LDPE was investigated by Py-GC/MS on a CDS analytics (Chemical Data Systems, Oxford, PA) 5200 series pyrolyser, close-coupled to a PerkinElmer Clarus 680 gas chromatograph (GC) and Clarus 600S mass spectrometer. A small amount of LDPE (approximately 0.7 mg) was placed inside a 25 mm quartz tube between quartz wool. For each catalytic experiment, the powdered polymer and powdered catalyst, with similar particle sizes (2-10 μm), were thoroughly mixed using a mortar and pestle until homogeneous to give a weight ratio of LDPE:catalyst = 3:1. A small mass of catalyst/LDPE mixture (approximately 1 mg) was pyrolysed.

For each experiment, the sample was heated by a platinum coil probe to 700 °C at 10 °C ms^{-1} with a hold time of 10 s under a He carrier gas flow. The pyrolysis interface was maintained at 290 °C to prevent prior condensation. Volatilised compounds were immediately trapped on a Tenax ®-TA adsorbent trap at 45 °C to avoid secondary/recombination reactions. The Tenax ®-TA adsorbent trap was then gradually heated to 295 °C over 2 mins and the pyrolysis products were transferred to the GC column via a heated transfer line kept at 310 °C. A PerkinElmer Elite-1701 column (cross-bond: 14% cyanopropylphenyl and 85% dimethyl polysiloxane; 30 m, 0.25 mm i.d., 0.25 mm df) was used to separate the products using helium as a carrier gas. The GC injection port was kept at 275 °C and a 1:125 split ratio was used. The GC oven was heated at 5 °C min^{-1} from 45 °C to 280 °C. Proposed peak assignments (m/z = 45-300) were made from mass spectra detection using the NIST 2011 MS library. The results are presented in area %, corresponding to the percentage area of the chromatogram peak with regards to the total peak area of the chromatogram. Thermal and catalytic Py-GC/MS experiments were performed in duplicate to confirm the reproducibility of the reported procedure.

Due to the elevated pyrolysis temperature, the thermal stability of the Al-SBA-15 catalysts was first confirmed by XRD after calcination at 700 °C at 1.5 °C min^{-1} for 5 h. The corresponding XRD patterns are displayed in the supporting information (Fig. S-2).

3. Results and discussion

3.1 Materials characterisation

Elemental analysis data of the Al-SBA-15 catalysts are given in Table 2. The experimentally determined Al content (given as Si/Al ratio) is close to the planned composition. This highlights the advantage of using the "pH-adjustment" method, which offers a high level of control of the incorporation of aluminium from the initial synthesis gel to the final solid, in agreement with prior work [16,27,29].

Table 2. Physicochemical properties of the studied catalysts.

Sample	Bulk Si/Al (at.)[a]	Surface Si/Al (at.)[b]	S ($m^2 g^{-1}$)[c]	V_μ ($cm^3 g^{-1}$)[d]	V_m ($cm^3 g^{-1}$)	V_T ($cm^3 g^{-1}$)[e]	d_p (nm)	Acid site loading (µmol g^{-1})	B (µmol g^{-1})	L (µmol g^{-1})	B/L
AlSBA15(5)	5	5	414	0.00	1.0	1.0	6.8	564	347	217	1.6
AlSBA15(15)	17	12	412	0.00	0.8	0.8	6.0	409	194	215	0.9
AlSBA15(35)	27	15	432	0.02	1.3	1.4	7.4	232	103	129	0.8
AlSBA15(100)	75	30	485	0.03	1.3	1.3	9.5	124	29	95	0.3
SBA-15	-	-	857	0.06	1.2	1.3	6.0	17	2	15	0.1
ZSM-5	12*	0.2	304	0.11	0.0	0.2	0.9	672	380	292	1.3

Determined by [a] ICP-OES, [b] XPS, [c] BET, [d] t-plot, [e] BJH, *commercial specification

XPS analysis of the catalysts shows a deviation of the Si/Al ratios on the surface compared to the bulk of the materials derived from ICP-OES (Table 2). The surface and bulk Si/Al ratio of the aluminium rich catalysts (nominal Si/Al = 5 and 15) are quite similar, suggesting that aluminium is uniformly dispersed within the SBA-15 structure. However, at higher Si/Al ratios (nominal Si/Al > 35), larger quantities of aluminium were found at the surface of the material, indicating that the aluminium is not homogeneously distributed throughout the material as was also noted in a previous study on the synthesis of ZSM-5 [38]. The increase in aluminium at the surface could possibly be due to extra-framework aluminium, leading to the generation of Lewis acid sites as opposed to Brønsted acid sites. Although an excess of Al in the synthesis procedure has not been investigated in this study, it can be assumed further incorporation of Al will lead to the formation of predominantly extra-framework Al.

Analysis of the Si 2p region in Fig. 2A shows a perturbation of the peaks to lower binding energies with increasing aluminium incorporation, attributed to the generation of Si-O-Al species in agreement with previous work [39]. The emergence of a peak at high aluminium levels is also evident at a binding energy of around 74 eV (Fig. 2B). This shifts slightly to higher binding energies, due to the formation of Si-O-Al species [40].

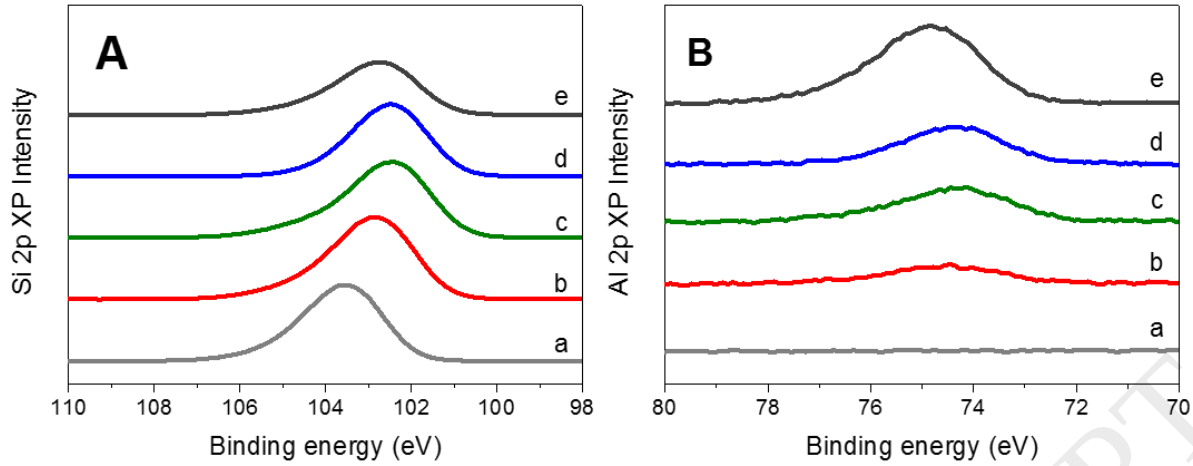

Fig. 2. High resolution XP spectra of (A) Si 2p and (B) Al 2p for Al-SBA-15 catalysts: (a) SBA-15, (b) AlSBA15(100), (c) AlSBA15(35), (d) AlSBA15(15) and (e) AlSBA15(5)

Fig. 3 shows the low-angle XRD patterns of the Al-SBA-15 catalysts and pure SBA-15, as a reference. The diffraction pattern in the low angle region displays an intense peak associated with the (100) plane and two less intense peaks associated with the (110) and (200) planes of the lattice. The diffraction patterns are all consistent with well-ordered 2D hexagonal structures typically displayed by SBA-15 mesoporous silica. A slight shift of the peak towards lower angles is evident in the (100) plane (B to D, Fig. 3 inset), due to an increase in lattice spacing (d). However, at the highest aluminium loading, i.e. AlSBA15(5), the angle of the peak is of similar value to the Al-free SBA-15 (a). The evidence of three distinct reflections in the low-angle XRD patterns in the series confirms that the short and long-range order of the hexagonal structure is unaffected by the incorporation of aluminium.

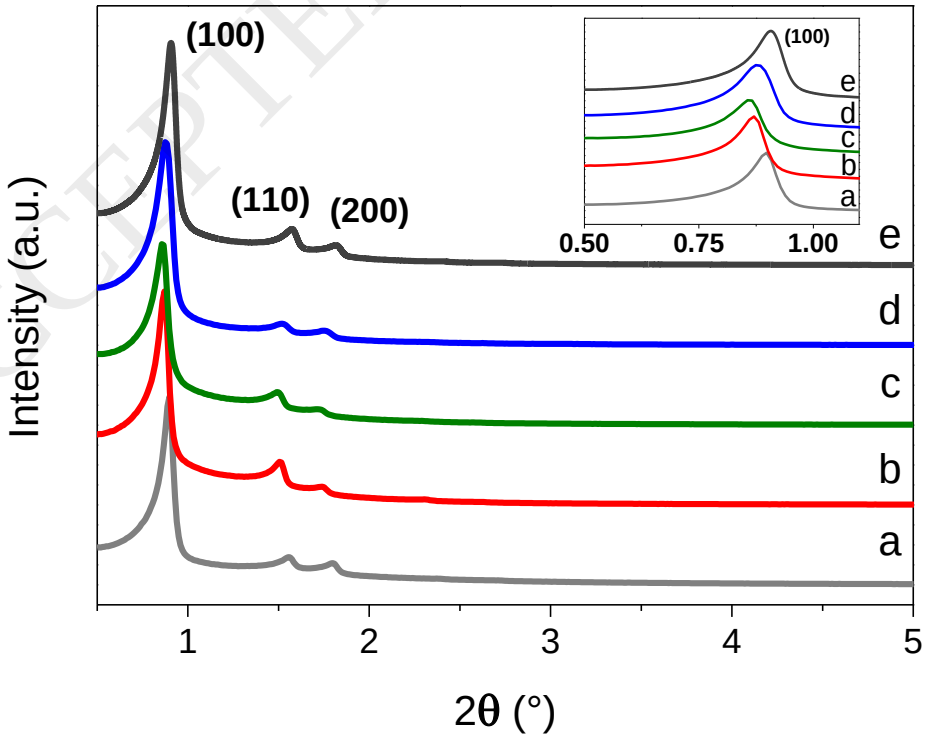

Fig. 3. Low angle XRD patterns of Al-SBA-15 catalysts: (a) SBA-15, (b) AlSBA15(100), (c) AlSBA15(35), (d) AlSBA15(15) and (e) AlSBA15(5) (inset: amplification of 2θ in the region between 0.5 and 1.1°).

The textural properties of the synthesised materials were analysed by N_2 physisorption (Fig. 4). All SBA-15 type catalysts exhibit type IV isotherms with H1 hysteresis, which are characteristic of mesoporous solids possessing cylindrical pore geometry and a high degree of pore size uniformity [41]. It appears that in the isotherms of the Al-SBA-15 catalysts with increasing aluminium content (b to e), the hysteresis loops are shifted to lower relative pressures, indicative of a decrease in pore sizes; with the exception of AlSBA15(5), having a similar pore size to the Al-free counterpart. At high Si/Al ratios (such as AlSBA15(35)), irregular hysteresis loops are evident, indicative of broad pore size distributions and large cylindrical pores. This is in agreement with the measurements obtained by XRD and indicate that structural ordering decreases at high Si/Al. Previous work by Ungureanu et al. [27], also noted an increase in structural ordering with a decrease in Si/Al. Their explanation for this observation was due to the addition of aluminium cations (from aluminium nitrate) in the synthesis solution. This resulted in increased ionic strength in the synthesis solution and hence a higher degree of ordering of the hexagonal structure of the SBA-15.

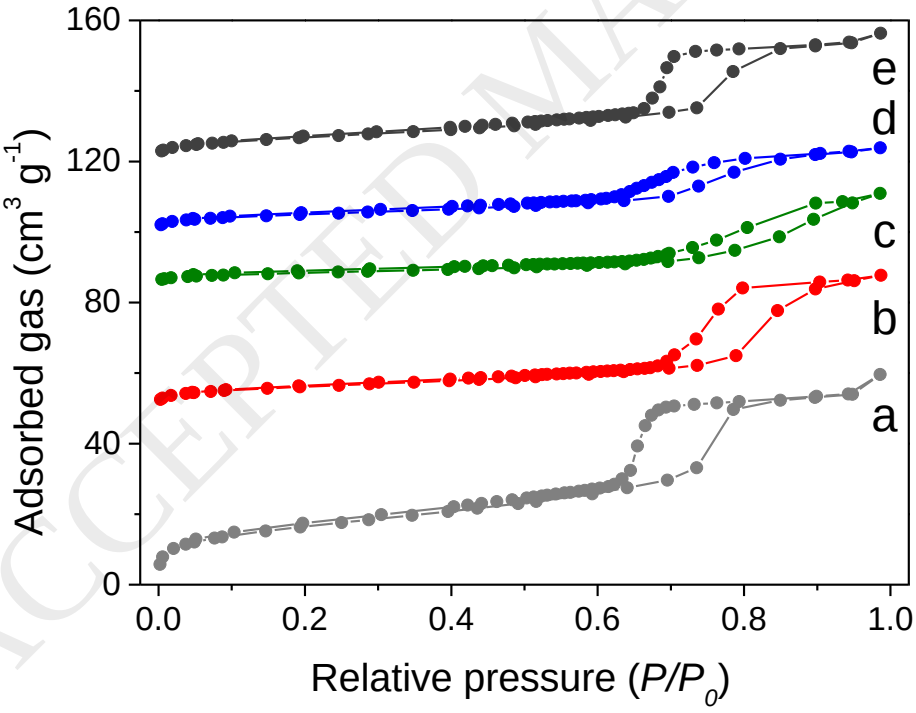

Fig. 4. N_2 physisorption isotherms of the Al-SBA-15 catalysts: (a) SBA-15, (b) AlSBA15(100), (c) AlSBA15(35), (d) AlSBA15(15) and (e) AlSBA15(5) (isotherms were offset for clarity).

The structural properties derived from the physisorption isotherms are summarised in Table 2 above. It is clear from the BET results that increasing the incorporation of aluminium dramatically decreases the surface area in the aluminium-rich catalysts compared with the Al-

free SBA-15. This is due to the disappearance of the micropore volume (V_μ) in the series, i.e. the micropores disappear with the increasing Al content; the Al-free material has a micropore volume of 0.06 $cm^3\ g^{-1}$ in comparison to 0.00 $cm^3\ g^{-1}$ for the AlSBA15(5) material. Hence, the introduction of Al species into the SBA-15 structure inhibits the formation of micropores in the synthesis. As such, micropore volume is below the detection limit for the AlSBA15(15) and AlSBA15(5) materials, therefore leading to a purely mesoporous material at higher Al concentrations.

Decreasing the Al content of the materials causes a slight decrease in the volume of mesopores (V_m) and total pore volume (V_T). On the other hand, the average pore (d_p) diameter of all the SBA-15 materials are in the region of 6-9 nm. These values are consistent with reported values in the literature for SBA-15 using similar preparation procedures [42–44]. It is worth noting that the pore diameter of the Al-rich materials appears to be larger than the Al-free SBA-15. The increase in pore diameter is associated with the longer hydrothermal treatment experienced by the Al-rich materials, which were treated for an additional 72 h in comparison to Al-free SBA-15 [45]. Fig. S-1 (in supporting information) shows the BJH pore size distributions of the Al-SBA-15 catalysts. SBA-15 exhibits the typical narrow pore size distribution centred at 6.0 nm. Incorporating Al up to a Si/Al ratio of 35 broadens the pore size distribution and shifts its centre to larger pore diameters. Further increase of the Al content (AlSBA15(5)) narrows the pore size distribution and centres at a lower diameter of 6.8 nm.

N_2 physisorption analysis of the ZSM-5 confirms the microporous nature of crystalline zeolite , with a micropore volume of 0.11 $cm^3\ g^{-1}$ and an average pore diameter of 0.9 nm, which is approximately an order of magnitude smaller than the Al-SBA-15 materials.

To further elucidate the structure of the Al-rich SBA-15 material, STEM was performed on AlSBA15(5). Fig. 5 shows well-ordered channels within the particle structure with an approximate length of 700-750 nm, which suggests that the reactant molecules will be travelling a substantial internal length of the mesopore whilst being exposed to the reactive acid sites. In addition to STEM, EDS analysis was also carried out. Fig. 6 shows EDS maps of the main elements (Si, O, and Al), confirming high dispersion of Al, Si and O atoms.

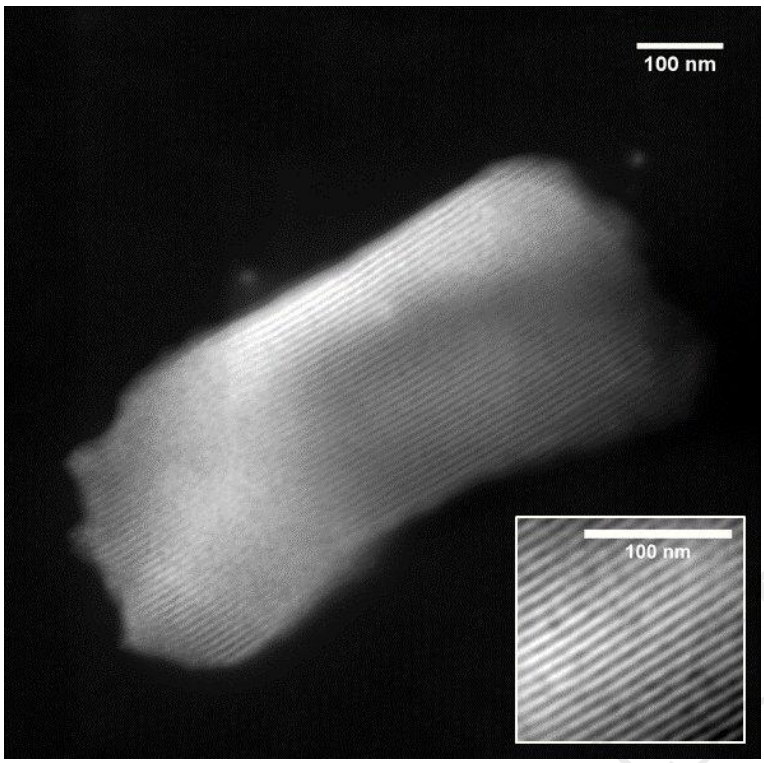

Fig. 5. High-resolution STEM image of an AlSBA15(5) particle. (Inset) increased magnification.

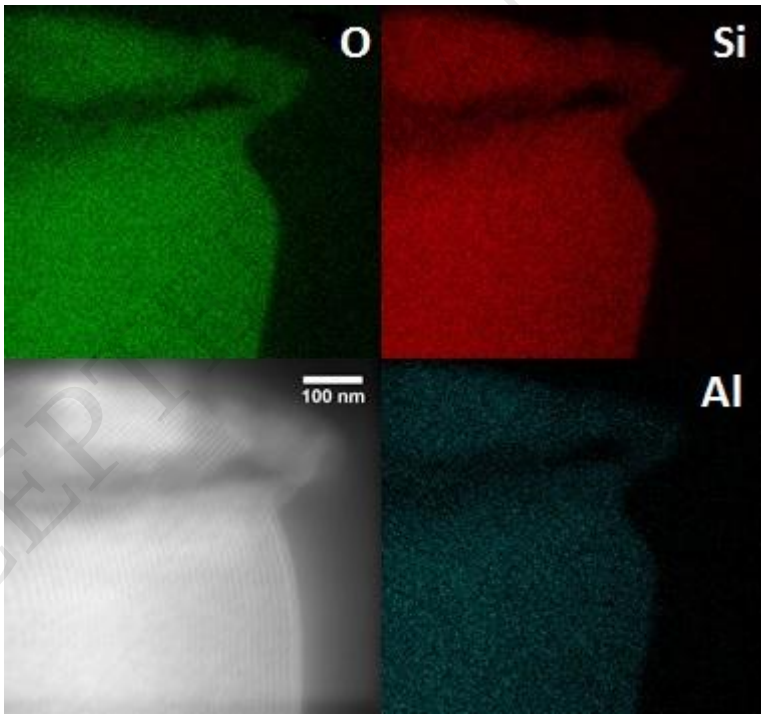

Fig. 6. Energy Dispersive X-Ray Spectroscopy (EDS) analysis of AlSBA15(5).

The acidic properties of all materials were investigated via n-propylamine chemisorption followed by TGA-MS analysis. N-propylamine is a weak base that reacts with accessible acid sites to form propene and ammonia under thermal conditions. The desorption temperature of reactively-formed propene is inversely proportional to the strength of the acid site. Fig. 7 shows that increasing the Al content of the material barely changes the propene desorption

temperature of 435 °C, suggesting that all the Al-SBA-15 materials possess acid sites of similar strength. In contrast to Al-SBA-15s, ZSM-5 exhibits two types of acid sites; strong acid sites (major peak centred at 407 °C) and weak acid sites (small peak centred at 473 °C). The acid site loadings were calculated and are presented in Table 2 above. The results show that the acid site loading closely mirrors the aluminium content of the catalysts. The aluminium species withdraw electrons from the framework hydroxyl groups, therefore increasing the dissociation capability of the proton [46]. A small number of acid sites were identified in SBA-15 which could be attributed to surface silanol groups. AlSBA15(5), with the highest aluminium incorporation, displays the highest total acidity which appears to be exponentially proportional to bulk aluminium incorporation as displayed in Fig. S-3.

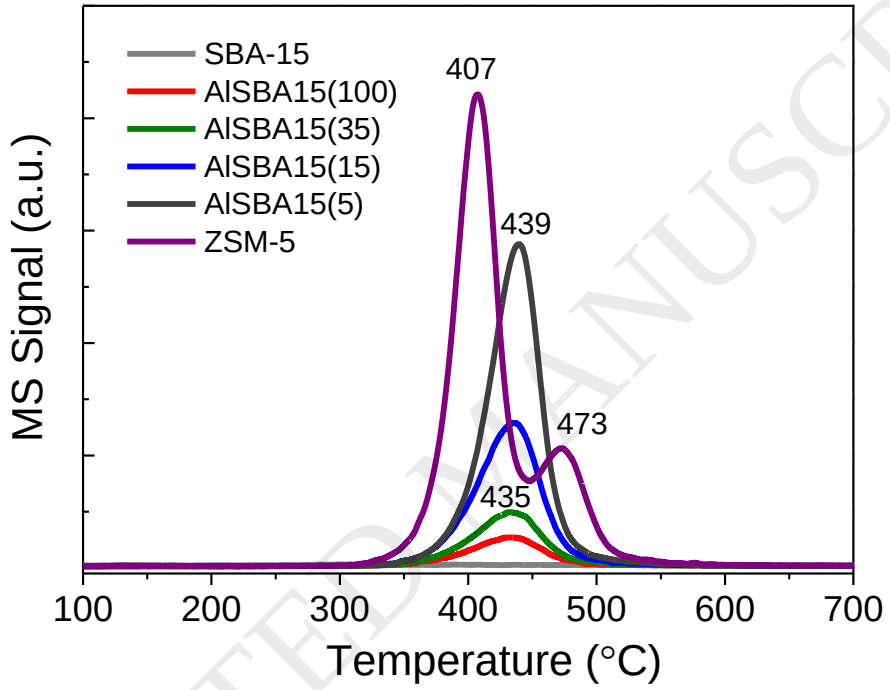

Fig. 7. Temperature programmed desorption of reactively formed propene from propylamine decomposition over Al-SBA-15 and ZSM-5 catalysts.

The adsorption of pyridine was studied using FTIR spectroscopy to assess the nature of the acid sites of the materials. The DRIFT spectra of the Al-SBA-15 catalysts and ZSM-5 zeolite, following chemisorption of pyridine, are shown in Fig. 8. Absorption features at 1445 and 1595 cm^{-1} are assigned to pyridine interacting by electron donation to Lewis acid sites, due to partially coordinated Al atoms in the extra-framework aluminium and silanol groups. This band is present in all samples and decreases in intensity with an increase in aluminium along the series of Al-SBA-15. An absorption band at 1545 cm^{-1} is more visible in AlSBA15(15), AlSBA15(5) and ZSM-5, which is commonly assigned to pyridinium ions (PyH^+) coordinated to a Brønsted acid site. The absorption band at 1490 cm^{-1} is assigned to pyridine adsorbed over Brønsted and Lewis sites [47]. The ratio of Brønsted to Lewis acidity present in the materials was calculated by integration of the 1445 and 1545 cm^{-1} absorption bands and are

presented in Table 2 above, along with the individual contributions. It is apparent that the Brønsted/Lewis ratio is positively correlated with the incorporation of aluminium, though a very small quantity of Brønsted and Lewis sites are present in the Al-free SBA-15. It is worth noting that 27Al NMR combined with acid site analysis on similar materials suggests that the Brønsted acid sites are generated by framework Al. Extra-framework Al typically led to Lewis acid sites [27].

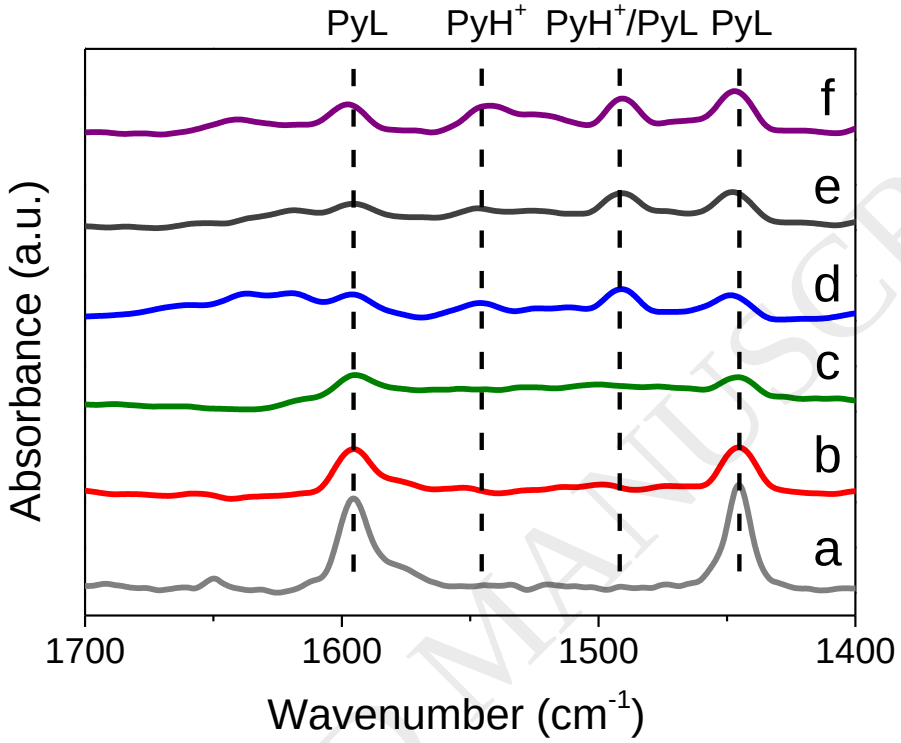

Fig. 8. DRIFT spectra of chemisorbed pyridine over Al-SBA-15 and ZSM-5 catalysts: (a) SBA-15, (b) AlSBA15(100), (c) AlSBA15(35), (d) AlSBA15(15), (e) AlSBA15(5) and (f) ZSM-5

TPD of ammonia is widely used for the characterisation of acid sites. However, due to the high basicity of ammonia, weak sites that may not contribute to the acidity of the catalyst are capable of being titrated. This can lead to an overestimation of the number of acid sites by this method. In addition, the small molecular size of ammonia enables the accessibility of all pores of the solid which may be impenetrable by larger molecules commonly found in cracking reactions [48]. In contrast, propyl amine, used in this study, gives a more realistic insight as it only titrates strong and medium strength acid sites. Furthermore, due to its larger size, it is only able to access pore sizes in the range required for catalytic cracking reactions.Therefore, the acid sites characterised in this study by propyl amine are all expected to be accessible and active in the cracking of LDPE.

In summary, the quantity of Brønsted acid sites generated in the Al-SBA-15 materials synthesised in this work is comparable with previously reported values where the “pH adjustment” method was employed. These observations highlight that the “pH adjustment”

method allows precise control over the incorporation of Al into the silica framework. Therefore, materials derived from this method afford acidic properties comparable to zeolites. It is worth noting, that the “pH adjustment” method is highly reproducible offering consistent results across studies.

3.2 Catalyst Testing

3.2.1 Thermogravimetric analysis

Thermogravimetric analysis was carried out to compare the activity of Al-SBA-15 catalysts with different Si/Al ratio on cracking of LDPE. Additionally, the protonic form of ZSM-5 (Alsi-Penta SM-27) with a nominal Si/Al of 12, was employed as a reference material.The results of the thermal and catalytic degradation of LDPE derived from thermogravimetric analysis are plotted in Fig. 9.

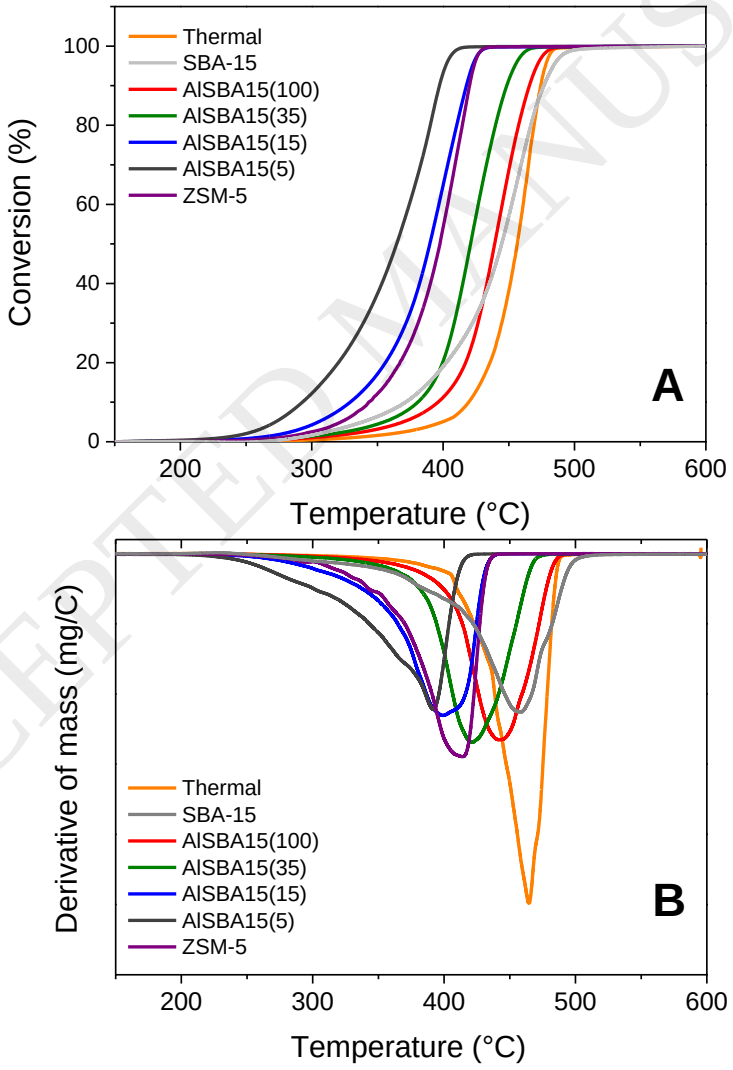

Fig. 9. (A) Conversion plot for the thermal and catalytic degradation of LDPE measured by thermogravimetric analysis. (B) Derivative thermogravimetric analysis plot of the thermal and catalytic degradation of LDPE.

Thermal degradation of pure LDPE polymer commenced around 400 °C, reaching a maximum reaction rate at 464 °C. In the presence of solid acid catalysts, the temperature of maximum degradation rate is shifted much lower due to the catalytic cracking over Brønsted acid sites [49]. The presence of pure SBA-15 causes a decrease of 7 °C to the temperature of maximum degradation rate suggesting that even with a low quantity of acid sites a noticeable catalytic effect is observed. Furthermore, Fig. 9 shows that LDPE degradation temperature decreases continuously with increasing Al loading of the catalyst. This can be attributed to the increasing Brønsted/Lewis acid site ratio. Fig. 10 shows temperatures of conversions at 5, 50 and 80%, derived from TGA data using Eq. 1, in relation to the Brønsted/Lewis ratio of the Al-SBA-15 catalysts. There is a clear linear correlation between the lower temperatures of LDPE degradation and increasing Brønsted acidity.

Since the Brønsted/Lewis ratio for the Al-SBA-15 catalysts increases with the incorporation of aluminium, a similar correlation can be seen for the number of acid sites. Nevertheless, it is difficult to distinguish the individual contribution of the two types of acid sites. However, based on the acidity analysis, it can be observed that the two Al-rich catalysts (AlSBA15(5) and AlSBA15(15)) possess very similar proportion of Lewis acid sites (Table 2) and similar acid strength (Fig. 7). Despite these similarities, the activity of AlSBA15(5) is considerably greater than that of AlSBA15(15) (Fig. 10 and Table S-1). Hence, the greater activity of AlSBA15(5) can be attributed to the higher Brønsted acid site loading. This hypothesis is supported by the literature, based on theoretical modelling performed by Li et al. [50], it was shown that Lewis acid catalysed cracking has a higher energy barrier compared to Brønsted acid cracking. Therefore, it can be concluded that both types of acid sites may contribute to the catalytic cracking of LDPE, however the contribution of Brønsted acid sites are more significant.

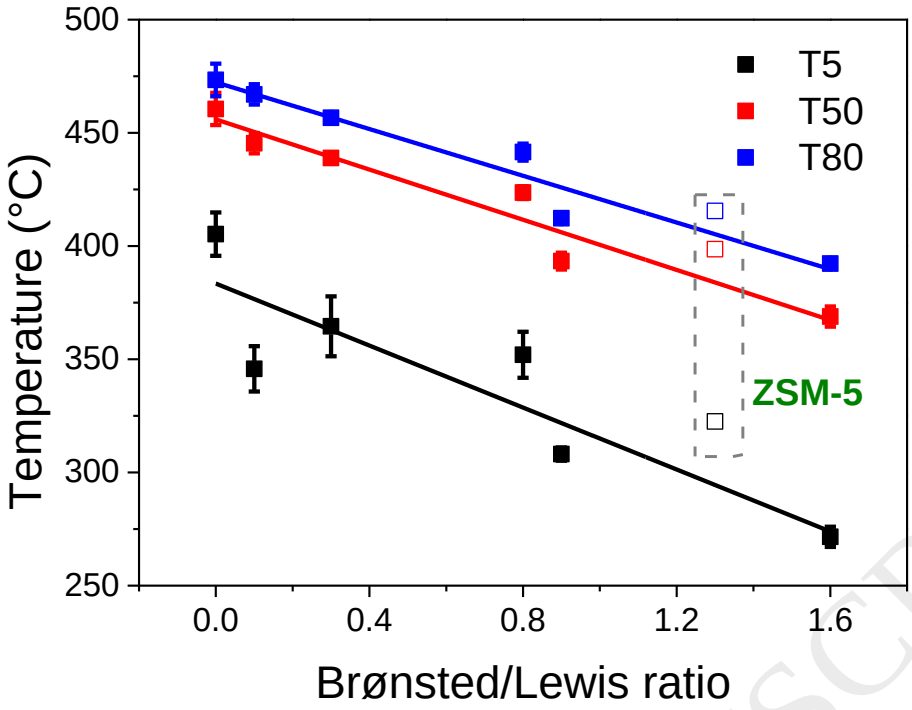

Fig. 10. Temperatures at conversions of 5, 50 and 80% of LDPE pyrolysis in relation to Brønsted to Lewis ratio of Al-SBA-15 catalysts and ZSM-5 (hollow squares).

An assessment of catalytic activity can be determined by a simple measurement of the temperature at which maximum cracking is observed (see Fig. 9B above), using thermogravimetric analysis. The catalyst lowers the activation energy of the cracking reaction; therefore, catalysts with higher activity perform maximum cracking at lower temperatures. As expected, ZSM-5 was highly active for the cracking reaction, due to its high acid site loading (672 μmol g^{-1}) and high Brønsted/Lewis ratio. However, ZSM-5 performed the degradation at a slightly higher temperature than the AlSBA15(15) catalyst, with a comparative Si/Al ratio, much higher than the AlSBA15(5) catalyst. This comparatively lower activity can be associated with the microporous nature of the ZSM-5 structure, which restricts the diffusion of sterically challenging molecules into its internal acid sites. This highlights the importance of evaluating a combination of increased Brønsted acidity and acid site accessibility for cracking sterically challenging molecules.

Previous investigations by Aguado et al. [5] into the catalytic degradation of LDPE, by a variety of catalysts, reported a maximum degradation rate at 396 °C using nanometer crystal-sized ZSM-5. A more recent investigation by Ding et al. [51], on the synthesis of mesoporous ZSM-5, reported a maximum degradation temperature of 348 °C, much lower than that of conventional ZSM-5. In this work, the lowest temperature of LDPE degradation was achieved with the AlSBA15(5), with a maximum degradation rate at around 390 °C. Therefore, it is clear the accessibility of the reactant molecules has a profound effect on the catalytic activity of the cracking of polyolefins. However, from a commercial perspective, the selectivity of the catalyst may be of more value, allowing the conversion to be tailored towards more desirable products.

3.2.2 Py-GC/MS analysis

Pyrolysis gas chromatography/mass spectroscopy (Py-GC/MS) was employed to investigate the distribution of the products i.e. the proportion of desired products compared to total products. The product distribution is highly dependent on pyrolysis temperature, heating rate and also on the occurrence of secondary reactions. A scheme of the reactor set-up is provided in Fig. 11. With the introduction of a volatile trap, secondary reactions are minimised due to the short residence time of the generated vapours. While this work was only able to consider volatile products with molecular weights below 300 g mol^{-1}, Py-GC/MS presents a simple analytical technique for the qualitative assessment of catalyst selectivity in LDPE catalytic pyrolysis.

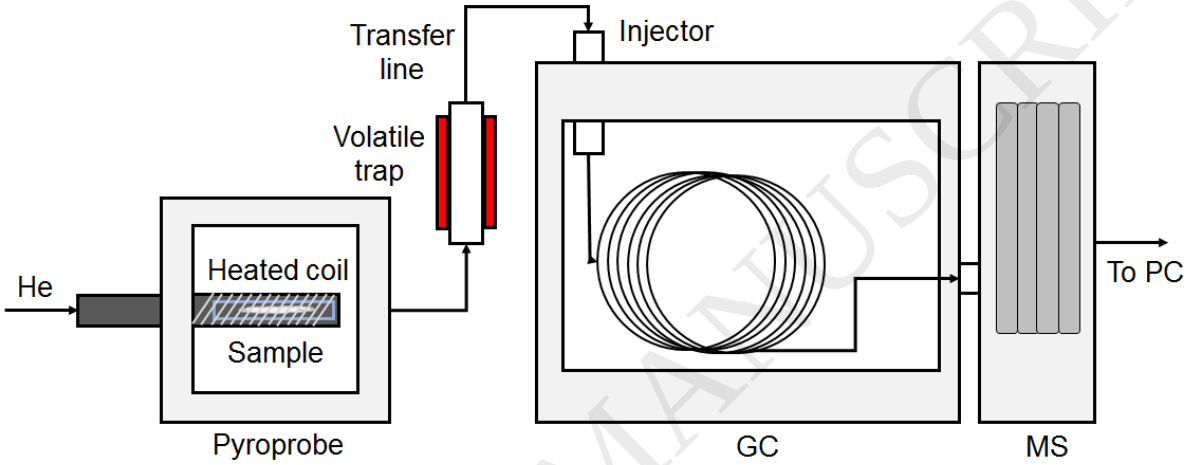

Fig. 11. Scheme of the pyroprobe reactor and GC/MS setup.

It is well known that the catalytic cracking of hydrocarbons is initiated through either the generation of a carbonium ion or a carbenium ion by a Brønsted or Lewis acid site, respectively, as shown in Fig. 12 [49]. However, due to the complexity of pyrolysis, with multiple reactions happening simultaneously, a more in depth reaction mechanism cannot yet be presented.

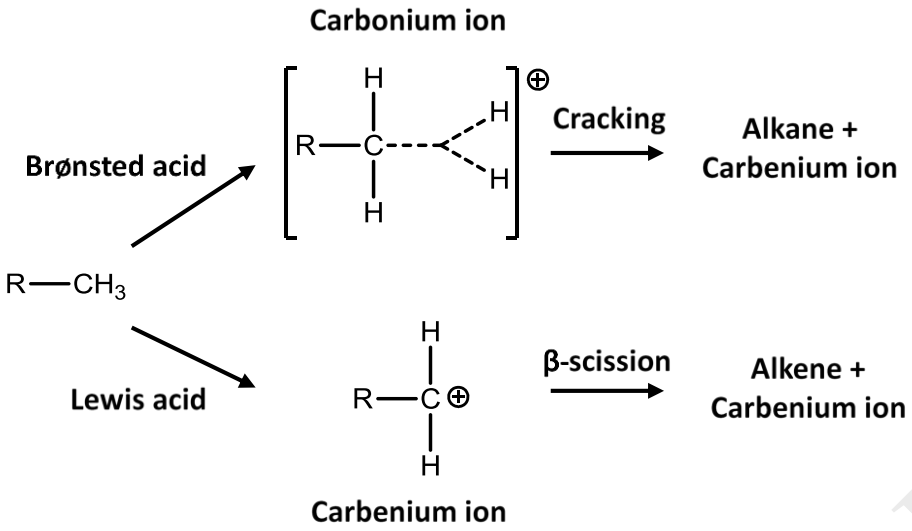

Fig. 12. Mechanism of acid catalysed cracking of hydrocarbons.

Fig. 13 shows the product distribution by the carbon number (C_n) of identifiable products, corresponding to the peak area % in the chromatogram, for the thermal and catalytic pyrolysis of LDPE as studied by Py-GC/MS (a more detailed breakdown is available in the supporting information, Fig. S-4). Characteristic triplet peaks are apparent in the GC chromatogram (see Fig. S-5), corresponding to the production of alkanes, alkenes and dienes. The molecules of each subsequent triplet peak contains an additional carbon atom as the peaks evolve. The product distribution of thermal LDPE pyrolysis yields a wide range of products spread between 4-20 C_n. Thermal pyrolysis mainly yielded C_7 products, this contributed to ca. 14 % of the overall identifiable products. Furthermore, as is evident in Fig. 13, the thermal pyrolysis of LDPE produced a higher percentage of products with longer carbon chain length ($C_{11\text{-}20}$) compared to the catalytic experiments.

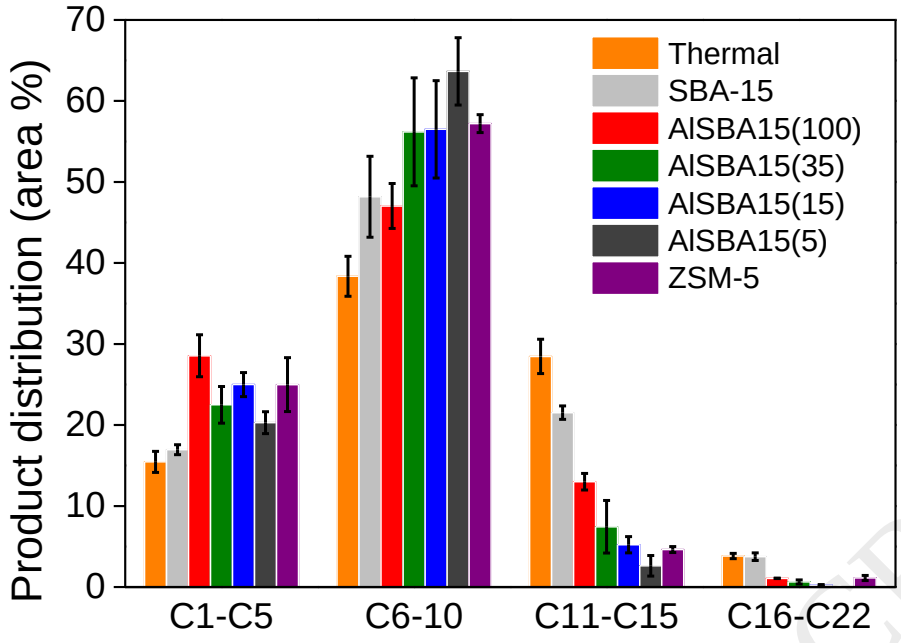

Fig. 13. The relative abundance of identified products from the thermal and catalytic cracking of LDPE analysed by Py-GC/MS, grouped by number of carbon atoms.

In the catalytic fast pyrolysis of LDPE at 700 °C, SBA-15 showed the least activity, with a selectivity similar to thermal pyrolysis, consistent with the low quantity of Brønsted and Lewis acid sites. Comparing the product distribution of LDPE cracking over SBA-15 with simple thermal cracking reveals that the selectivity to small hydrocarbon compounds with $1 < C_n < 10$ has slightly increased while lowering the selectivity of Cn > 10 products.

Critically, the product distribution from the catalytic cracking of LDPE appears to depend strongly on the Al content of the SBA-15 materials. In other words, by tuning the Al content of SBA-15 the selectivity of the LPDE catalytic cracking can be altered, directing the reaction towards a different range of products. The results in Fig. 13 show that with increased aluminium content of the Al-SBA-15 catalysts, a higher degree of cracking is achieved. More specifically, increasing the Al content of the materials lead to a significant reduction in the formation of $C_n > 10$ products in favour of forming $C_n < 10$ compounds in the range of gasoline (C_6-C_{12}), as shown in Fig. 13. At increased aluminium incorporation (Si/Al < 35), there was a complete absence of the characteristic triplicate peak corresponding to an alkane, alkene and diene in the GC chromatogram. This suggests that the typical products from thermal cracking of LDPE are further cracked or converted in the presence of strong acid catalysts. This led to an irregular product distribution for each catalyst, dependent on individual catalyst selectivity.

ZSM-5 also resulted in a high level of cracking, reducing the number of products with $C_{11\text{-}22}$, and increasing the number of lower C_n products, particularly between $C_{7\text{-}8}$. Interestingly, ZSM-5 displayed a greater percentage of aromatic products in comparison to the Al-SBA-15 catalysts. This is due to its shape-selective ability from its complementary pore size and

structure [1,52]. This suggests that shape selectivity is much more important for the production of aromatics than acidity, although low acidity in the Al-SBA-15s appeared to be preferential for the production of aromatics (Fig. S-4, C_{6-8}). Furthermore, although ZSM-5 had a much higher acidity than AlSBA15(15), it produced a similar distribution of products in the region of C_{11-22} to the AlSBA15(15) catalyst. Again, this could be due to the microporous nature of the material and thus the diffusional hindrances of the long-chained polymers in comparison to the mesoporous SBA-15 type materials.

Based on the Py-GC/MS analysis, it is evident the degree of LDPE cracking is a function of aluminium loading and in particular the quantity of Brønsted acidity. Hence, Al-rich SBA-15 materials produced predominantly short chain-length products, greater than that of ZSM-5. Therefore, due to the increased pore size and increased achievable acidities of Al-SBA-15, comparable to that of zeolites, the application of these catalysts for the catalytic cracking of sterically challenging feedstocks is promising. However, it is evident that ZSM-5 is highly shape selective towards the production of aromatics, preventing further cracking to lower molecular weight molecules. This presents an opportunity for further investigation into a multi-step catalytic approach, with high acidity mesoporous catalysts being initially used to crack the bulky feedstock molecules followed by ZSM-5 to produce aromatics. Research is underway to identify quantifiable product yields and to investigate scale-up challenges of Al-SBA-15 such as catalyst lifetime and reusability and also to investigate a close coupled sequential process.

Conclusions

In summary, a series of Al-SBA-15 catalysts were synthesised and applied to the catalytic cracking of bulky polyolefin molecules, LDPE, and compared to ZSM-5. The product distribution from the catalytic cracking of LDPE depends strongly on the Al content of the SBA-15 materials. The maximum rate of catalytic LDPE degradation (calculated by thermogravimetric analysis) was achieved by AlSBA15(5), with a Si/Al of 5, approximately 70 °C lower than that of simple thermal degradation. The catalytic activity of all the synthesised Al-SBA-15 catalysts was demonstrated to be directly proportional to acidity and, more specifically, Brønsted to Lewis ratio. Due to the enhanced diffusional efficiency of reactants in the mesoporous structure of the Al-SBA-15 catalysts compared to ZSM-5, a higher selectivity of molecules in the gasoline range was produced in the case of AlSBA15(5) as demonstrated by Py-GC/MS analysis. Moreover, the pore architecture of the catalyst had a significant effect on the product selectivity. The micropore openings of ZSM-5 were more selective towards aromatic products, preventing further cracking while the Al-SBA-15 materials allow for a broader distribution of aliphatic products. In conclusion, high acidity Al-SBA-15 catalysts are promising for the catalytic cracking of sterically challenging feedstocks such as waste plastics. This work paves the way for the development of sequential reactor systems which include

efficient catalytic cracking units followed by catalytic upgrading of the resultant catalytic pyrolysis products.

Acknowledgements

Joseph Socci would like to gratefully acknowledge Aston University for financing his PhD scholarship. The authors would also like to acknowledge Jinsen Tian from the School of Metallurgy and Materials, University of Birmingham for his assistance with STEM-EDS measurements. Amin Osatiashtiani and Georgios Kyriakou would like to thank The British Council for funding through the Newton Institutional Links scheme.

References

[1] D.P. Serrano, J. Aguado, J.M. Escola, ACS Catal. 2 (2012) 1924–1941.
[2] G. Manos, A. Garforth, J. Dwyer, Ind. Eng. Chem. Res. 39 (2000) 1198–1202.
[3] D.P. Serrano, J. Aguado, J.M. Escola, J.M. Rodríguez, G. San Miguel, J. Anal. Appl. Pyrolysis 74 (2005) 370–378.
[4] A. Marcilla, A. Gómez, S. Menargues, J. García-Martínez, D. Cazorla-Amorós, A. Gó Mez, S. Menargues, J. García-Martínez, D. Cazorla-Amorós, J. Anal. Appl. Pyrolysis (2003) 495–506.
[5] J. Aguado, D.P. Serrano, G.S. Miguel, J.M. Escola, J.M. Rodríguez, J. Anal. Appl. Pyrolysis 78 (2007) 153–161.
[6] J. Čejka, G. Centi, J. Perez-Pariente, W.J. Roth, Catal. Today 179 (2012) 2–15.
[7] A. Taguchi, F. Schu, F. Schüth, Microporous Mesoporous Mater. 77 (2005) 1–45.
[8] M. Kruk, M. Jaroniec, Y. Sakamoto, O. Terasaki, R. Ryoo, C.H. Ko, J. Phys. Chem. B 104 (2000) 292–301.
[9] J. Iglesias, J.A. Melero, G. Morales, M. Paniagua, B. Hernández, A. Osatiashtiani, A.F. Lee, K. Wilson, Catal. Sci. Technol. 8 (2018) 4485–4493.
[10] R. Huirache-Acuña, R. Nava, C. Peza-Ledesma, J. Lara-Romero, G. Alonso-Núez, B. Pawelec, E. Rivera-Muñoz, Materials (Basel). 6 (2013) 4139–4167.
[11] J.C. Manayil, C.V.M. Inocencio, A.F. Lee, K. Wilson, Green Chem. (2015) 1–6.
[12] J.C. Manayil, A. Osatiashtiani, A. Mendoza, C.M.A. Parlett, M.A. Isaacs, L.J. Durndell, C. Michailof, E. Heracleous, A. Lappas, A.F. Lee, K. Wilson, ChemSusChem 10 (2017) 3506–3511.
[13] Y. Li, W. Zhang, L. Zhang, Q. Yang, Z. Wei, Z. Feng, C. Li, J. Phys. Chem. B 108 (2004) 9739–9744.
[14] S. Chen, J. Li, Y. Zhang, Y. Zhao, K. Liew, J. Hong, Catal. Sci. Technol. 4 (2014) 1005.
[15] L. Lizama, T. Klimova, J. Reyes, O. Gutie, O. Gutiérrez, L. Lizama, Appl. Catal. A Gen. 335 (2008) 159–171.
[16] S. Wu, Y. Han, Y.C. Zou, J.W. Song, L. Zhao, Y. Di, S.Z. Liu, F.S. Xiao, Chem. Mater. 16 (2004) 486–492.
[17] Z. Luan, M. Hartmann, D. Zhao, W. Zhou, L. Kevan, Chem. Mater. 11 (1999) 1621–1627.
[18] S. Sumiya, Y. Oumi, T. Uozumi, T. Sano, J. Mater. Chem. 11 (2001) 1111–1115.
[19] S. Zeng, J. Blanchard, M. Breysse, Y. Shi, X. Shu, H. Nie, D. Li, Microporous Mesoporous Mater. 85 (2005) 297–304.
[20] W. Hu, Q. Luo, Y. Su, L. Chen, Y. Yue, C. Ye, F. Deng, Microporous Mesoporous Mater. 92 (2006) 22–30.
[21] R. Van Grieken, J.M. Escola, J. Moreno, R. Rodríguez, Appl. Catal. A Gen. 305 (2006) 176–188.
[22] G. Muthu Kumaran, S. Garg, K. Soni, M. Kumar, J.K. Gupta, L.D. Sharma, K.S. Rama Rao, G. Murali Dhar, Microporous Mesoporous Mater. 114 (2008) 103–109.

[23] B. Dragoi, E. Dumitriu, C. Guimon, A. Auroux, Microporous Mesoporous Mater. 121 (2009) 7–17.
[24] J.M.R. Gallo, C. Bisio, G. Gatti, L. Marchese, H.O. Pastore, Langmuir 26 (2010) 5791–5800.
[25] P. Bhange, D.S. Bhange, S. Pradhan, V. Ramaswamy, Appl. Catal. A Gen. 400 (2011) 176–184.
[26] A.J.J. Koekkoek, J.A. Rob van Veen, P.B. Gerrtisen, P. Giltay, P.C.M.M. Magusin, E.J.M. Hensen, Microporous Mesoporous Mater. 151 (2012) 34–43.
[27] A. Ungureanu, B. Dragoi, V. Hulea, T. Cacciaguerra, D. Meloni, V. Solinas, E. Dumitriu, Microporous Mesoporous Mater. 163 (2012) 51–64.
[28] S. Lin, L. Shi, T. Yu, X. Li, X. Yi, A. Zheng, Microporous Mesoporous Mater. 207 (2015) 111–119.
[29] D. Meloni, D. Perra, R. Monaci, M.G. Cutrufello, E. Rombi, I. Ferino, Appl. Catal. B Environ. 184 (2016) 163–173.
[30] S. Xing, P. Lv, J. Fu, J. Wang, P. Fan, L. Yang, Z. Yuan, Microporous Mesoporous Mater. 239 (2017) 316–327.
[31] C.O. Arean, M.R. Delgado, P. Nachtigall, H.V. Thang, M. Rubeš, R. Bulánek, P. Chlubná-Eliášová, Phys. Chem. Chem. Phys. 16 (2014) 10129.
[32] Y. Yue, A. Gédéon, J.-L. Bonardet, J.-B. D'Espinose, J. Fraissard, N. Melosh, Chem. Commun. (1999) 1967–1968.
[33] J.M. Escola, D.P. Serrano, M. Arroyo, A. Alba, J. Mater. Cycles Waste Manag. 16 (2014) 435–441.
[34] K. Li, S.W. Lee, G. Yuan, J. Lei, S. Lin, P. Weerachanchai, Y. Yang, J.-Y. Wang, K. Li, S.W. Lee, G. Yuan, J. Lei, S. Lin, P. Weerachanchai, Y. Yang, J.-Y. Wang, Energies 9 (2016) 431.
[35] A. Corma, Chem. Rev. 95 (1995) 559–614.
[36] M.A. Uddin, K. Koizumi, K. Murata, Y. Sakata, Polym. Degrad. Stab. 56 (1997) 37–44.
[37] D. Zhao, J. Feng, Q. Huo, N. Melosh, G. Fredrickson, B. Chmelka, G. Stucky, Science (80-.). 279 (1998) 548–52.
[38] R. Borade, A. Sayari, A. Adnot, S. Kaliaguine, J. Phys. Chem. 94 (1990) 5989–5994.
[39] C.M.A. Parlett, L.J. Durndell, A. Machado, G. Cibin, D.W. Bruce, N.S. Hondow, K. Wilson, A.F. Lee, Catal. Today 229 (2014) 46–55.
[40] A. Osatiashtiani, B. Puértolas, C.C.S. Oliveira, J.C. Manayil, B. Barbero, M. Isaacs, C. Michailof, E. Heracleous, J. Pérez-Ramírez, A.F. Lee, K. Wilson, Biomass Convers. Biorefinery 7 (2017) 331–342.
[41] M. Kruk, M. Jaroniec, Chem. Mater. 13 (2001) 3169–3183.
[42] J. Fan, C. Yu, L. Wang, B. Tu, D. Zhao, Y. Sakamoto, O. Terasaki, J. Am. Chem. Soc. 123 (2001) 12113–12114.
[43] M. Hartmann, A. Vinu, Langmuir 18 (2002) 8010–8016.
[44] S.S. Kim, A. Karkamkar, T.J. Pinnavaia, M. Kruk, M. Jaroniec, J. Phys. Chem. B 105 (2001) 7663–7670.
[45] P.F. Fulvio, S. Pikus, M. Jaroniec, J. Mater. Chem. 15 (2005) 5049–5053.
[46] R. Carvajal, P.-J. Chu, J.H. Lunsford, J. Catal. 125 (1990) 123–131.
[47] D.P. Serrano, R.A. García, G. Vicente, M. Linares, D. Procházková, J. Čejka, J. Catal. 279 (2011) 366–380.
[48] J. Čejka, A. Corma, S. Zones, Zeolites and Catalysis, 2010.
[49] H. Zhang, Y. Ma, K. Song, Y. Zhang, Y. Tang, J. Catal. 302 (2013) 115–125.
[50] Q. Li, K.C. Hunter, A.L.L. East, J. Phys. Chem. A 109 (2005) 6223–6231.
[51] J. Ding, J. Hu, T. Xue, Y. Wang, H. Wu, P. Wu, M. He, RSC Adv. 6 (2016) 38671–38679.
[52] H. Zhang, Y.-T. Cheng, T.P. Vispute, R. Xiao, G.W. Huber, Energy Environ. Sci. 4 (2011) 2297.